ADVANCES IN FOREST FIRE RESEARCH

2022

Edited by
DOMINGOS XAVIER VIEGAS
LUÍS MÁRIO RIBEIRO

A Study of the Ignition Mechanism for Dead Pinus Palustris Needles

Weixuan Gong*; Juan Cuevas; Albert Simeoni

Department of Fire Protection Engineering, Worcester Polytechnic Institute, MA 01605, USA, {wgong@wpi.edu}

**Corresponding author*

Keywords

Wildfire, Ignition criterion, Pyrolysis gas evolution, Modified Cone Calorimeter, FTIR spectrometry

Abstract

Combinations of cumulative impacts of drought, invasive species, climate variability, and ever-expanding wildland-urban interface make landscapes more susceptible to devastating wildland fires. To treat the increasing risks of wildland fires, one of the ways is to mitigate the risk of ignition, which requires a solid understanding of the ignition mechanism of vegetation fuels. This can be achieved mainly through discerning the degradation stage and the ignition criteria. Scaling up the experiments for the degradation stage and evaluating the suitability of existing ignition criteria are two of the primary challenges for ignition studies on vegetation fuels.

Motivated by the challenges, two series of experiments were conducted using a modified Cone Calorimeter to understand the mechanisms driving the ignition of dead Pinus palustris needles. In the first set of experiments, the ignition of pine needles was studied for varied incident heat fluxes (20-35 kW/m2) and air flow rates (buoyancy-induced - 100 l/min forced flow). In the second set of experiments, Fourier transform infrared spectroscopy (FTIR) was used to characterize the composition of the pyrolysis gases generated from the thermal degradation of pine needles when exposed to various incident heat fluxes (20 and 30 kW/m2) under an inert atmosphere obtained using a flow of pure nitrogen.

The results for the first series of experiments show that the critical mass loss rate at ignition increase with both flow rates and heat flux. From the second set of experiments, it was found that methane (CH4), carbon monoxide (CO), carbon dioxide (CO2), and water vapor (H2O) are the main constituents of the pyrolysis gases. The predominance of these compounds was found to be independent of the external heat flux while their concentrations are sensitive to it. The flammability of pyrolysis gas was found to increase with external heat flux.

1. Introduction

There is an urgent need to advance wildland fire management due to the increasing risk of wildfires (Richer et al., 2006). One of the ways to reduce the risk of wildfires is to avoid ignition, which requires a solid understanding of the occurrence of the flaming combustion of the vegetation fuels.

Characterizing the pyrolyzing process and the ignition moment are the two primary challenges of understanding the ignition of wildland fuels. Mass-loss kinetics and pyrolysis gas characterization are the focuses of pyrolyzing process research. Although the mass loss kinetics has been well studied on a micro-scale experimental basis (Leroy et al., 2010; Liu et al., 2002), it is necessary to scale up the experiments while maintaining fuel properties. For the pyrolysis gas aspect, the technology for identifying the components is advanced (Nunes et al., 2018), while there is a gap in quantifying the dynamics of each component over time.To characterize the occurrence of ignition, the condensed-phase criteria, including ignition temperature, critical mass loss rate, and heat release rate at ignition are widely accepted. However, the suitability of these criteria needs to be checked and verified because of the broad ranges of these values reported by the literature.(Delichatsios, 2020; Lyon & Quintiere, 2007)

Motivated by the challenges, the objectives of this work are dual. The first is to explore the influence of external heat flux on the pyrolysis process of dead Pinus palustris needles. The evolution of pyrolysis gas is expected to be characterized and quantified by FTIR spectroscopy. The second one is to investigate the relationships between a solid-phase ignition criterion and different experimental conditions.

2. Materials and Experimental Design

2.1. Experimental Design

A modified cone calorimeter, shown in Figure 1, was used to study the pyrolysis and ignition mechanisms of pine needles.

Two series of experiments were conducted to understand the mechanisms driving the ignition of dead Pinus palustris needles. In the first set of experiments, FTIR spectroscopy was used to characterize the composition of the pyrolysis gases generated from the thermal degradation of pine needles when the fuel bed was exposed to incident heat fluxes of 20 and 30 kW/m^2, and a nitrogen inflow of 50 l/min being fed from the bottom of the combustion chamber. The main constituents of the pyrolysis gas were identified by the characteristic bands shown in FTIR scans and were quantified by applying Beer-Lambert's law (Plummer, Reagen & Logan, 2003).

In the second set of experiments, the ignition of pine needles was studied for incident heat fluxes ranging from 20 to 35 kW/m^2 and air inflows of 0 l/min to 100 l/min. In these tests, the time-to-ignition (t_{ig}), and the critical mass-loss rate at ignition ($\dot{m}''_{cr}$) were evaluated.

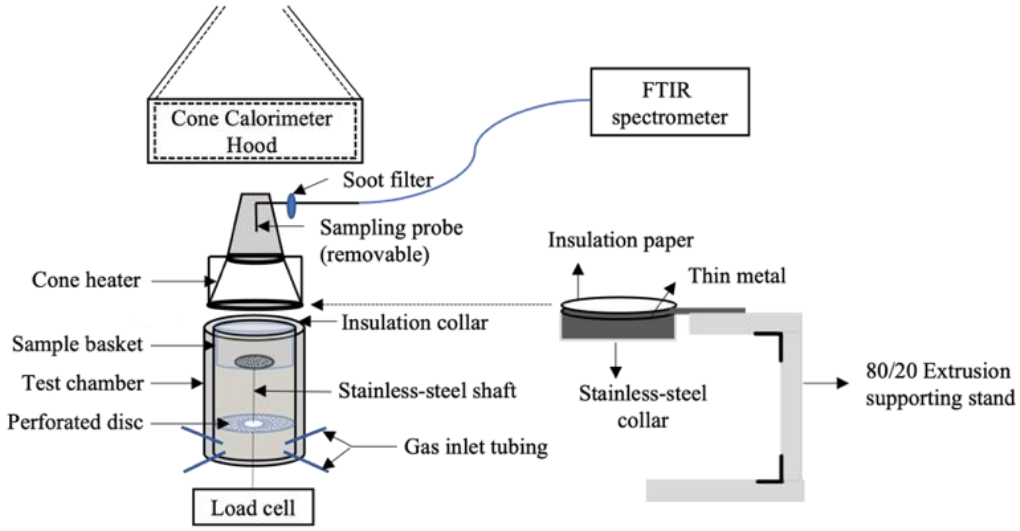

Figure 1 – Experimental apparatus: modified cone calorimeter allowing the inflow with desired flow rates

2.2. Materials

The fuel samples were oven-dried at 60°C for 24 h for conditioning and measuring their residual moisture content. After this, the conditioned pine needles were stored in sealed containers until testing. All the samples had an average fuel moisture content of 4.6 % on a dry weight basis.

For the experiments, 20 g of conditioned pine needles were placed in a cylindrical sample holder 12.6 cm in diameter and 3 cm in depth. Two different types of sample holders, shown in Figure 2, were used; for the experiments with no inflow of oxidizer being fed through the bottom of the combustion chamber (buoyancy-induced flow), a sample holder with 0% porosity was used. For experiments with a forced inflow being supplied, a sample holder with 63% porosity was used.

(a) (b)

Figure 2 - Fuel samples for the tests with (a) buoyancy-induced flow using the basket of 0% opening and (b) forced flow using the basket of 63% opening.

3. Results and Discussion

3.1. FTIR analysis of pyrolysis gas

3.1.1. Pyrolysis gas component identification

Figure 3 presents the FTIR spectra of the pyrolysis gas samples collected during the experiments conducted at 20 kW/m^2 and 30 kW/m^2, respectively. The main constituents of the pyrolysis gas determined by the characteristic bands shown in FTIR scans include CH_4, CO, CO_2, and H_2O. The characteristic bands at 2880-3180 cm^{-1}, 2010-2250 cm^{-1}, and 2290-2390 cm^{-1} indicate the formation of CH_4, CO, and CO_2. The characteristic bands at 1390-2020 cm^{-1} and 3500-3998 cm^{-1} represent the occurrence of H_2O. Similar pyrolysis gas components of plant species are also found in other literature (Granada et al., 2012).

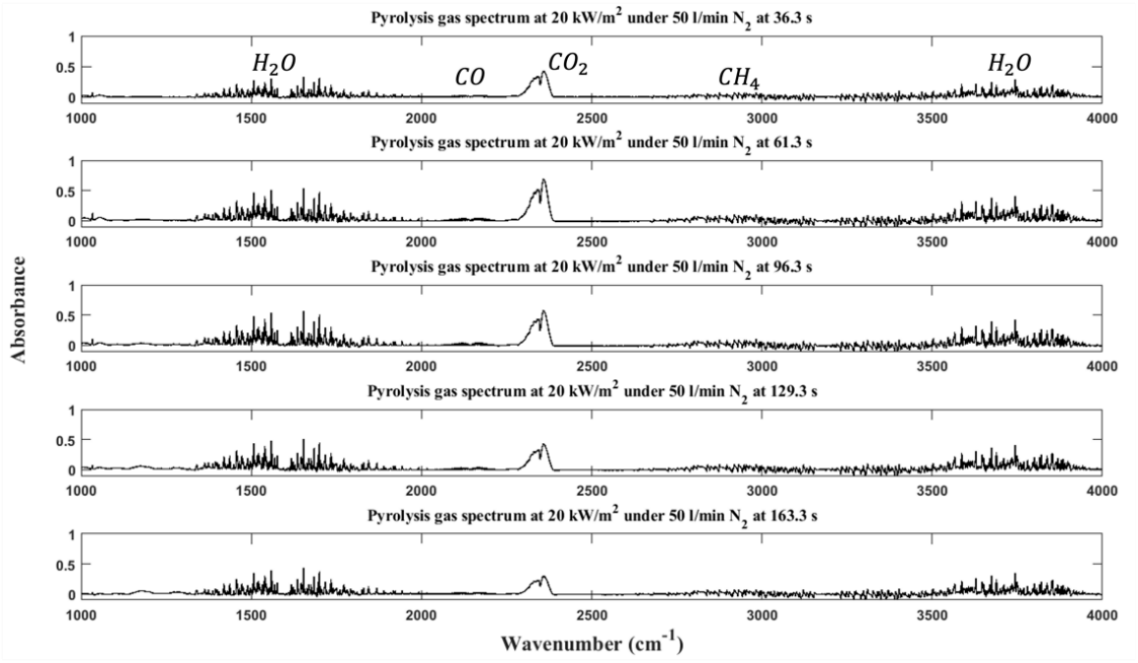

(a)

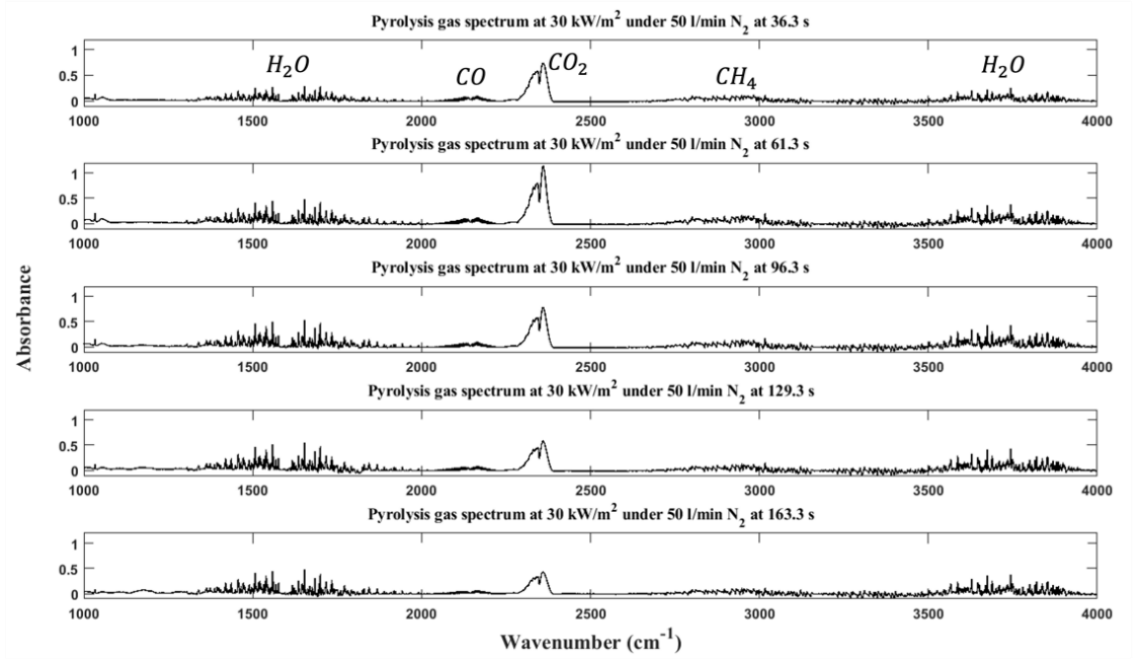

(b)

Figure 3 - Pyrolysis gas FTIR spectra at 50 l/min N_2 and (a) 20 kW/m^2, 50 l/min N_2 and (b) 30 kW/m^2.

3.1.2. Quantification of the pyrolysis gas constituents

Figure 4 shows the evolution of the concentration of the different gas species identified in the pyrolysis gas samples collected at both heat flux levels. All the results are averaged from three repetitions. It is essential to highlight that the calculated concentration of each component at each moment is not the instantaneous concentration at that moment, but the average concentration over time of the data collection (26.3 s).

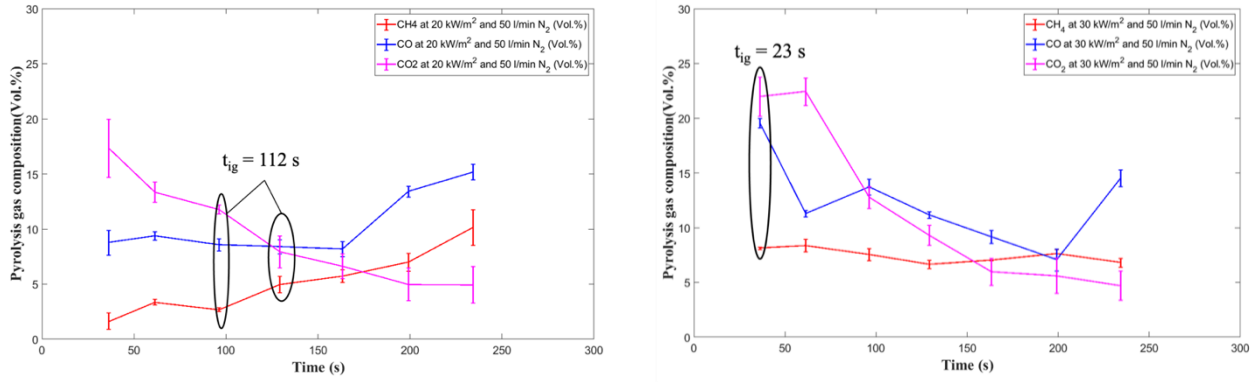

(a) ***(b)***

Figure 4 - Pyrolysis gas concentration evolution at 50 l/min N2 and (a) 20 kW/m2, 50 l/min N2 and (b) 30 kW/m2.

Combining these results with the time-to-ignition under the same conditions (see Section 3.2), it is possible to evaluate the composition of the pyrolysis gases at ignition. For an incident heat flux of 20 kW/m^2, the concentration of CH_4, CO, CO_2, and H_2O at ignition are found to be 3.8, 8.5, 9.9, and 77.8 vol.%. For an incident heat flux of 30 kW/m^2, the concentrations of CH_4, CO, CO_2, and H_2O at ignition are 8.1, 19.6, 22.0, and 44.1 vol.%.

Thus, the effective heat of combustion of the pyrolysis gases (H_{c_py}) can be evaluated as the weighted sum of the heat of combustion of each species, defined by Eqs. (1) and (2).

$$H_{c\_py} = Y_{CO} \cdot H_{c\_CO} + Y_{CH_4} \cdot H_{c\_CH_4} \quad \text{Eq (1)}$$

$$Y_i = \frac{X_i M_i}{\sum X_i M_i} \quad \text{Eq (2)}$$

where X_i, M_i, Y_i, and H_{c_i} are the mole fraction, molecular weight, mass fraction, and heat of combustion of a given gas species. The reference values of the heat of combustion of CH_4 and CO are 50.1 and 10.1 kJ/g, respectively (Quintiere, 2006).

The resulting effective heat of combustion of the pyrolysis gases was evaluated to be 2.6 kJ/g and 6.4 kJ/g for 20 and 30 kW/m^2, respectively. This result is in general agreement with the range of values (from 4.62 to 5.38 kJ/g) reported by (Cancellieri et al., 2005). The variation of the heat of combustion on different heat fluxes indicates that the pyrolysis gas obtained at a higher heat flux is of greater flammability.

3.2. Ignition tests(tig)

3.2.1. Time-to-ignition (tig)

Table 1 presents the mean ignition time (t_{ig}), mean thermal penetration depth (δ), and dimensionless thermal depth (x) measured at external heat fluxes ranging from 20 to 35 kW/m^2, and airflow rates of 0, 50, and 100 l/min air.

Table 1: Mean time-to-ignition, thermal penetration depth, and dimensionless thermal depth for a 30 mm fuel bed under different external heat fluxes and flow rates.

Flow rate (l/min)	Heat flux (kW/m^2)	t_{ig} (s)	δ (mm)	x (-)
0	20	66.67 (3.54)	9.16 (0.25)	3.28 (0.09)
	25	19.33 (3.76)	4.88 (0.43)	6.28 (0.50)
	30	13.00 (0.82)	4.04 (0.12)	7.44 (0.22)
	35	5.67 (0.27)	2.67 (0.07)	11.26 (0.28)
50	20	124.33 (18.47)	12.39 (1.04)	2.48 (0.23)
	25	35.67 (9.06)	6.51 (0.92)	4.95 (0.81)
	30	22.67 (2.37)	5.32 (0.28)	5.68 (0.29)
	35	12.33 (2.76)	3.87 (0.43)	8.01 (0.80)
100	20	No ignition	-	-
	25	88.67 (5.18)	10.56 (0.27)	2.85 (0.07)
	30	38.33 (3.17)	6.92 (0.34)	4.36 (0.21)
	35	20.00 (2.41)	4.98 (0.35)	6.10 (0.39)

The thermal penetration depth, defined in Eq. (3), represents the depth pyrolysis layer (Delichatsios, 2020). The dimensionless thermal depth is defined as the ratio of the fuel sample thickness to the thermal penetration depth (Delichatsios, 2020), and it is used to discriminate whether the fuel bed shows thermally-thick or thermally-thin behavior at ignition based on the criterion presented in Eq. (4) (M. Delichatsios, 2020).

$$\delta = \sqrt{\alpha t_{ig}} \qquad \text{Eq (3)}$$

$$x = \frac{\tau}{\delta} = \begin{cases} < 0.8 & thermally\ thin \\ 0.8 < x < 2 & thermally\ intermediate \\ 2 < & thermally\ thick \end{cases} \qquad \text{Eq (4)}$$

For a thermal diffusivity of pine needles (α) of 1.26 × 10-6 m^2/s (Korobeinichev et al., 2018), it appears that the 30 mm-thick pine needle bed behaves thermally thick for all testing conditions.

From the table, it can be seen that t_{ig} and δ increase when increasing the airflow rate and decrease when increasing the magnitude of the external incident heat flux over the fuel bed. When increasing airflow rates, the net heat delivered to the fuel bed decreases due to an enhanced convective cooling through the fuel bed, which reduces the pyrolysis reaction rate of the fuel bed and the quantity of the released fuel vapor. Meanwhile, the generated fuel vapor through the pyrolysis is diluted by the incoming airflow.

On the other hand, the decrease of t_{ig} and δ when increasing the external incident heat flux over the fuel bed is due to the steepness of the temperature profile developed inside the fuel bed; higher incident heat fluxes will increase the amount of energy available to promote the pyrolysis reaction, increasing its rate. Thus, less time is required until a sufficient fuel rate for ignition is achieved. Furthermore, higher incident heat fluxes will produce steeper temperature profiles, causing a decrease in the relative distance between the thermal propagation depth and the pyrolysis front depth. Thus, as the time-to-ignition decreases with the magnitude of the external heat flux, the thermal wave can only propagate into depths closer to the surface of the fuel bed.

3.3. Critical mass loss rate ($\dot{m}''_{cr}$)

The results of the critical mass-loss rate **($\dot{m}''_{cr}$)** are shown in Figure 5. The uncertainties of the results are determined by one standard deviation of three repetitions for each test.

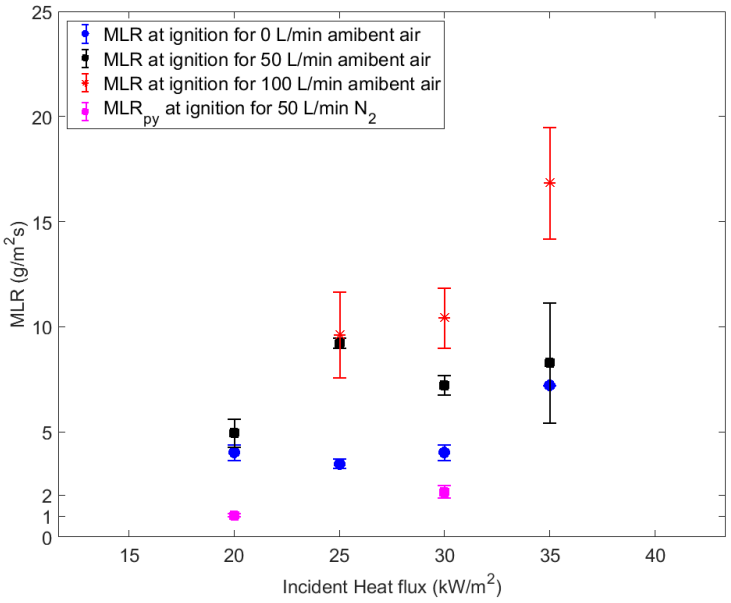

Figure 5 – Critical mass loss rate (MLR) for sustained flaming ignition

The critical mass-loss rate at ignition was found to increase when increasing the external incident heat flux and the airflow rate. Two mechanisms mainly drive the mass loss of the fuel bed. One part of the mass loss is due to pyrolysis, while the other one is due to the smoldering combustion of the fuel bed. Both reactions have been found to increase their rate when provided more energy (Bartlett & Bisby, 2015). Thus, increasing the magnitude of the external incident heat flux over the fuel bed increases the pyrolysis rate, smoldering combustion, and consequently, the mass-loss rate of the fuel bed. The reason for the increase of $\dot{m}''_{cr}$ when increasing the airflow rate is due to the dilution of the flammable mixture. As the chemical reaction at flaming ignition is near stoichiometric (Lyon & Quintiere, 2007), the fuel vapor concentration needs to increase with the airflow rates so that the equivalence ratio meets the requirements for ignition. Therefore, to obtain sufficient fuel, as shown in Eq (5), the thermal depth or the pyrolysis reaction rate needs to be increased. The increase in thermal depth with airflow rates has been shown in the analysis in 3.2.1. The pyrolysis reaction rate can also be locally increased by the appearance of smoldering spots, which is consistent with the observation that smoldering was detected before ignition for all tests conducted under forced flow conditions.

4. Conclusion

The work presented herein attempted to enhance our understanding of the conditions that lead to the ignition of Pinus palustris pine needles through a series of experiments aimed at characterizing the pyrolysis gases and the conditions under which piloted ignition occurs.

In pyrolysis tests, the influence of different heat fluxes on pyrolysis gas yields was investigated. The yield, generation rate, and flammability of pyrolysis gas were all found to increase with increasing heat fluxes.

In ignition tests, the influences of external heat fluxes and airflow rates on the time to ignition and mass loss rate at ignition were analyzed. The analysis of time-to-ignition results indicated that the thermal behavior of the fuel bed at ignition was influenced by both heat fluxes and airflow rates. The analysis of mass loss rate suggested significant contributions of smoldering combustion to the flaming ignition under low heat fluxes and high airflow rate conditions.

5. References

Bartlett, A., & Bisby, L. A. (2015). Analysis of cross-laminated timber upon exposure to non-standard heating conditions Structural behaviour of cross-laminated timber elements in fires View project FireComp View project. https://www.researchgate.net/publication/270875737

Cancellieri, D., Leoni, E., & Rossi, J. L. (2005). Kinetics of the thermal degradation of Erica arborea by DSC: Hybrid kinetic method. Thermochimica Acta, 438(1–2), 41–50. https://doi.org/10.1016/j.tca.2005.07.013

Delichatsios, M. (2020). Effects of material thickness on ignition times and creeping flame spread in the thermal regime: Theory, analytical solution and experimental justification. Fire Safety Journal, 116. https://doi.org/10.1016/j.firesaf.2020.103204

Granada, E., Eguía, P., Vilan, J. A., Comesaña, J. A., & Comesaña, R. (2012). FTIR quantitative analysis technique for gases. Application in a biomass thermochemical process. Renewable Energy, 41, 416–421. https://doi.org/10.1016/j.renene.2011.11.020

Korobeinichev, O. P., Shmakov, A. G., Osipova, K. N., Kumar, A., & Kambam Meetei, N. (2018). Experimental Study and Numerical Modeling of Downward Flame Spread Along a Single Pine Needle: Part 1 (Experiments). Combustion Science and Technology, 190(1), 164–185. https://doi.org/10.1080/00102202.2017.1380001

Leroy, V., Leoni, E., & Cancellieri, D. (2010). Thermal Degradation of Lignocellulosic Fuels: Biopolymers Contribution. In Biopolymers. Sciyo. https://doi.org/10.5772/10267

Liu, N. A., Fan, W., Dobashi, R., & Huang, L. (2002). Kinetic modeling of thermal decomposition of natural cellulosic materials in air atmosphere. In Journal of Analytical and Applied Pyrolysis (Vol. 63). www.elsevier.com/locate/jaap

Lyon, R. E., & Quintiere, J. G. (2007). Criteria for piloted ignition of combustible solids. Combustion and Flame, 151(4), 551–559. https://doi.org/10.1016/j.combustflame.2007.07.020

Ningbo, G., Baoling, L., Aimin, L., & Juanjuan, L. (2015). Continuous pyrolysis of pine sawdust at different pyrolysis temperatures and solid residence times. Journal of Analytical and Applied Pyrolysis, 114, 155–162. https://doi.org/10.1016/j.jaap.2015.05.011

Nunes, L. J. R., de Oliveira Matias, J. C., & da Silva Catalão, J. P. (2018). Applications for Torrefied Biomass. In Torrefaction of Biomass for Energy Applications (pp. 203–214). Elsevier. https://doi.org/10.1016/b978-0-12-809462-4.00011-0

Plummer, G., M., Reagen, W., K., & Logan, P., W. (2003). Organic and inorganic gases by extractive FTIR spectrometry. NIOSH Manual of Analytical Methods, Fourth Edition. https://www.cdc.gov/niosh/docs/2003-154/pdfs/3800.pdf

Richer, H. B., Anderson, J., Brewer, J., Davis, S., Fahlman, G. G., Hansen, B. M. S., Hurley, J., Kalirai, J. S., King, I. R., Reitzel, D., Rich, R. M., Shara, M. M., & Stetson, P. B. (2006). Probing the faintest stars in a globular star cluster. Science, 313(5789), 936–940. https://doi.org/10.1126/science.1130691

Setchkin, N. P. (n.d.). A Method and Apparatus for Determining the Ignition Characteristics of Plastics.